INTERNATIONAL JOURNAL OF CLIMATOLOGY, VOL. 13, 347–370 (1993) 551.513.1:551.588.6(71)

CLASS—A CANADIAN LAND SURFACE SCHEME FOR GCMS, II. VEGETATION MODEL AND COUPLED RUNS

D. L. VERSEGHY, N. A. McFARLANE AND M. LAZARE
Canadian Climate Centre, 4905 Dufferin Street, Downsview, Ontario M3H 5T4, Canada

Received 3 April 1992
Accepted 28 July 1992

ABSTRACT

In the companion to the present paper, the soil model associated with CLASS (Canadian Land Surface Scheme) was outlined. In this paper, the accompanying vegetation model is described. This model includes physically based treatment of energy and moisture fluxes from the canopy as well as radiation and precipitation cascades through it, and incorporates explicit thermal separation of the vegetation from the underlying ground. Seasonal variations of canopy parameters are accounted for. The morphological characteristics of the 'composite canopy' associated with each grid square are calculated as weighted averages over the vegetation types present. Each grid square is divided into a maximum of four separate subareas: bare soil, snow-covered, vegetation-covered, and snow-and-vegetation covered.

Test runs were done in coupled mode with the Canadian Climate Centre GCM, to evaluate the performance of CLASS compared with that of the simpler land surface scheme previously used. Two versions of CLASS were run: one with ponded surface water saved between time steps, and one with it discarded. For the seasons of June–July–August and December–January–February, diagnostic calculations showed that the old scheme underestimated the globally averaged land surface screen temperature by as much as 3·0°C, and overestimated the globally averaged precipitation rate over land by up to 1·0 mm day^{-1}. CLASS, on the other hand, produced screen temperature anomalies, varying in sign, of 0·2–0.3°C, and positive precipitation anomalies of 0·6–0·7 mm day^{-1}. The relatively poor performance of the old model was attributed to its neglect of vegetation stomatal resistance, its assumption that the contents of the soil moisture 'bucket' had to be completely frozen before the surface temperature could fall below 0°C, and its use of the force-restore method for soil temperatures, which systematically neglects long-term thermal forcing from the soil substrate. The assumption made in most GCMs that excess surface water immediately becomes overland runoff is shown to result in substantial overestimates of surface screen temperatures in continental interiors.

KEY WORDS Land surface processes General circulation models Canadian land surface scheme Climate modelling

1. INTRODUCTION

In the companion to the present paper (Verseghy, 1991), the soil model associated with CLASS (Canadian Land Surface Scheme) was described, and was shown to simulate a more physically realistic soil thermal and hydrological regime than the model that had been used to date in the Canadian Climate Centre GCM (incorporating the force-restore method for the calculation of soil temperatures and the so-called 'bucket' model for soil moisture). In this paper, the treatment of vegetation in CLASS is outlined, and the performance of the complete model is evaluated.

Vegetation canopies have been shown to exert a profound influence on surface fluxes of heat and moisture. The effects of canopy interception on surface evaporation rates, stomatal resistance on transpiration rates, and rooting depth on the supply of soil moisture available for transpiration were demonstrated by Warrilow *et al.* (1986). The last two are recognized as being particularly important; for example, Meehl and Washington (1988) showed that the sensitivity of soil moisture to climate change in doubled-CO_2 experiments was largely controlled by the amount of soil moisture present in the control run. Improvements in the simulation of certain aspects of land surface climate have been noted when more physically realistic land surface schemes are coupled to GCMs (e.g. Sato *et al.*, 1989; Sud *et al.*, 1990).

0899–8418/93/040347–24$17.00

Vegetation models developed for use in GCMs generally follow one of three strategies. Some adopt the approach of lumping together the canopy and ground and assuming the calculated surface temperature to apply to the vegetation as well as to the soil (e.g. Carson, 1986; Abramopoulos *et al.*, 1988; Noilhan and Planton, 1989). Others use a form of the model proposed by Deardorff (1978), which treats the vegetation canopy in effect like a 'big leaf', and applies an averaged vertical flux transfer coefficient to the entire grid square (e.g. Dickinson *et al.*, 1986; Taconet *et al.*, 1986; Tjernström, 1989). One or two approach the vegetation layer from first micrometeorological principles, assuming a homogeneous, semi-infinite canopy (e.g. Sellers *et al.*, 1986). However, most models, particularly the more complex ones, assume that each GCM grid square is a monoculture, i.e. that the entire vegetation cover consists of the single most frequently occurring vegetation type.

The vegetation model associated with CLASS is similar to some of the above models in that it treats the vegetation cover as a single layer, based on the approach attributed to Monteith (e.g. Thom and Oliver, 1977). However, rather than assuming that only one biome is present on each grid square, it calculates average canopy parameters based on the different vegetation types present. Furthermore, because turbulent transfers of energy and momentum are strongly and non-linearly dependent on local atmospheric stability and surface roughness (e.g. Mahrt, 1987), each grid square is divided into four separate subareas: bare soil, snow-covered, vegetation-covered and vegetation-and-snow covered, which are treated independently. (Similar strategies are adopted by Avissar and Pielke (1989) and Carlson *et al.* (1990), in schemes developed for mesoscale models and remote sensing purposes respectively.) These and other aspects of the model are discussed below, and the results of parallel test runs are presented with CLASS and the old model coupled in turn to the Canadian Climate Centre GCM.

2. OUTLINE OF CLASS VEGETATION MODEL

In CLASS, four broad vegetation groups are recognized within the canopy-covered subareas of each grid square: needleleaf trees, broadleaf trees, crops and grass. Each of these vegetation types is characterized by a distinctive form of canopy architecture. They are therefore treated separately, and their effects are averaged to obtain 'composite canopy' values of albedo, transmissivity, roughness length, unstressed stomatal resistance, standing mass, rooting depth, etc.

2.1. Radiation fluxes

The radiative properties of vegetation differ considerably for visible and near-infrared radiation, since the absorptivity of plant surfaces is high in the photosynthetically active, visible range but drops rapidly at longer wavelengths. The albedo and transmissivity of vegetation canopies can also show a marked dependence on the angle of incoming radiation. CLASS therefore uses different strategies to treat the incoming visible and near-infrared radiation under clear and cloudy skies.

Canopy albedo theoretically varies with both zenith angle Z of incoming radiation and the average leaf angle distribution $\bar{O}$. Following the analysis of Goudriaan (1988), the all-wave canopy albedo of a given vegetation type under clear skies can be written approximately as:

$$\alpha_c = \frac{2\bar{O}}{\bar{O} + \cos Z_s} \alpha_{c,H} \tag{1}$$

where $\alpha_{c,H}$ is the all-wave albedo the canopy would exhibit if all of its leaves were horizontal, and Z_s is the solar zenith angle. For trees, field observations show that diurnal variations in total albedo, and thus its dependence on solar zenith angle, are slight. This occurs in the case of needleleaf trees because of the clumping of leaves in various orientations and because of the conical shape of individual trees, both of which lead to a high degree of canopy roughness and consequent radiation trapping at all angles. In the case of broadleaf trees, the preferred orientation of leaves tends to be horizontal, so that $\bar{O} = \cos Z_s$ and $\alpha_c = \alpha_{c,H}$. For trees in general, therefore, the instantaneous values of visible and near-infrared albedoes are simply taken to

be equal to their average observed values:

$$\left.\begin{aligned}\alpha_{c,\,VIS} &= \bar{\alpha}_{c,\,VIS} \\ \alpha_{c,\,NIR} &= \bar{\alpha}_{c,\,NIR}\end{aligned}\right\} \text{(trees)} \qquad \begin{matrix}(2a)\\(3a)\end{matrix}$$

Under leafless conditions, different values are specified for the two cases of snow-covered or snow-free ground under the canopy. The canopy albedo remains at its fully-leafed value until half of the leaves have fallen; thereafter, it varies linearly with leaf area index down to the appropriate leafless value.

For crops, the assumption of a spherical leaf angle distribution has been found to be a reasonable one. (In the absence of suitable field measurements, the same assumption is made for natural grasses.) In such cases, $\bar{O}=0{\cdot}5$, and from equation (1), α_c is proportional to $(0{\cdot}5+\cos Z_s)^{-1}$. A perusal of the literature reveals that for clear skies, with $\cos Z_s < 0{\cdot}5$, $\alpha_{c,H}$ is well approximated by the average total canopy albedo $\bar{\alpha}_c$. For $\cos Z_s \geqslant 0{\cdot}5$, the value of α_c calculated using $\bar{\alpha}_c$ underestimates the measured canopy albedo; a better approximation is obtained by averaging the value so obtained with $\bar{\alpha}_c$ itself. Thus, the all-wave canopy albedo for clear skies, $\alpha_{c,\odot}$, is given by

$$\left.\begin{aligned}\alpha_{c,\odot} &= \frac{\bar{\alpha}_c}{0{\cdot}5+\cos Z_s}, && \cos Z_s < 0{\cdot}5 \\ \alpha_{c,\odot} &= \bar{\alpha}_c\left[0{\cdot}5+\frac{1}{1+2\cos Z_s}\right], && \cos Z_s \geqslant 0{\cdot}5\end{aligned}\right\} \text{(crops and grass)} \qquad (4)$$

The canopy albedo for cloudy skies, $\alpha_{c,\otimes}$, is simply approximated as $\bar{\alpha}_c$:

$$\alpha_{c,\otimes} = \bar{\alpha}_c \quad \text{(crops and grass)} \qquad (5)$$

For partly cloudy skies, interpolation between the two values is done according to the relative magnitudes of the fluxes of incident direct and diffuse radiation, $K_{\downarrow D}$ and $K_{\downarrow d}$:

$$\alpha_c = \frac{\alpha_{c,\odot}K_{\downarrow D}+\alpha_{c,\otimes}K_{\downarrow d}}{K_{\downarrow D}+K_{\downarrow d}} \qquad \text{(crops and grass)} \qquad (6)$$

The total canopy albedo, α_c, is partitioned into its visible and near-infrared components by assuming that since leaves absorb strongly in the visible portion of the spectrum, canopy albedos will be small in this range, and can be assumed to vary negligibly on a diurnal time-scale. Thus, for crops and grass as well as for trees, the visible albedo is assigned its average value:

$$\alpha_{c,\,VIS} = \bar{\alpha}_{c,\,VIS} \qquad \text{(crops and grass)} \qquad (2b)$$

The near-infrared albedo can then be obtained as a residual, from the total and visible canopy albedos and the incident visible and near-infrared fluxes $K_{\downarrow VIS}$ and $K_{\downarrow NIR}$:

$$\alpha_{c,\,NIR} = \frac{\alpha_c[K_{\downarrow VIS}+K_{\downarrow NIR}]-\alpha_{c,\,VIS}K_{\downarrow VIS}}{K_{\downarrow NIR}} \qquad \text{(crops and grass)} \qquad (3b)$$

For crops and grass, since the leaf area index Λ is not allowed to fall below 1 (see section 2.5 below), albedos retain their fully leafed values for all values of Λ except when the ground below the canopy is snow-covered. In this case, different (constant) values of $\alpha_{c,\,VIS}$ and $\alpha_{c,\,NIR}$ are specified, using as a first approximation the values assigned to leafless trees with an underlying snow cover.

Finally, if there is snow stored on the canopy itself, field measurements show (Leonard and Eschner, 1968) that the canopy albedo does not take on the high values associated with a fresh snow pack, but rather reaches a maximum of 0·20. In this case, canopy albedos are recalculated as averages of this snow-covered value and the snow-free values evaluated as above, weighted according to the snow stored on the canopy relative to the maximum moisture storage capacity (see section 2.3 below).

Radiation transmission within the canopy is a much stronger function of zenith angle than albedo and furthermore is dependent on leaf area index, since for a complete canopy cover, reflection back to the

atmosphere originates near the vegetation tops, whereas transmission is controlled by the bulk canopy structure. The total transmissivity τ_c of the canopy is calculated using a form of Beer's law of radiation transfer in non-scattering media:

$$\tau_c = \exp(-\kappa\Lambda) \tag{7}$$

where κ, the extinction coefficient, is calculated as

$$\kappa = \frac{\varepsilon \bar{O}}{\cos Z} \tag{8}$$

and ε is a correction factor less than or equal to 1, accounting for forward-scattering of radiation and non-random leaf distributions (i.e. clumping). For crops and grass, as noted above, and also for needleleaf trees, the distribution of leaf angles is assumed to be spherical; thus, $\bar{O} = 0{\cdot}5$. For broadleaf trees, as previously noted, $\bar{O} = \cos Z$. In the case of clear skies, consultation of numerous sources for appropriate values of ε produced the following relations for κ for the four main canopy types:

$$\kappa_{\odot} = 0{\cdot}3/\cos Z_s \quad \text{(needleleaf trees)} \tag{9a}$$

$$\kappa_{\odot} = 0{\cdot}4 \quad \text{(broadleaf trees, full canopy)} \tag{9b}$$

$$\kappa_{\odot} = 0{\cdot}8/\cos Z_s \quad \text{(broadleaf trees, leafless)} \tag{9c}$$

$$\kappa_{\odot} = 0{\cdot}4/\cos Z_s \quad \text{(crops and grass)} \tag{9d}$$

In the visible range, scattering is less important because of high leaf absorptivities. Thus, for visible radiation, larger values of ε are found than for the total solar spectrum. The following results were obtained for the four vegetation types:

$$\kappa_{\odot,\mathrm{VIS}} = 0{\cdot}4/\cos Z_s \quad \text{(needleleaf trees)} \tag{10a}$$

$$\kappa_{\odot,\mathrm{VIS}} = 0{\cdot}7 \quad \text{(broadleaf trees, full canopy)} \tag{10b}$$

$$\kappa_{\odot,\mathrm{VIS}} = 0{\cdot}8/\cos Z_s \quad \text{(broadleaf trees, leafless)} \tag{10c}$$

$$\kappa_{\odot,\mathrm{VIS}} = 0{\cdot}5/\cos Z_s \quad \text{(crops and grass)} \tag{10d}$$

The clear-sky transmissivity of the canopy for near-infrared radiation is calculated as a residual, using an equation analogous to (3b):

$$\tau_{c,\odot,\mathrm{NIR}} = \frac{\tau_{c,\odot}[K_{\downarrow\mathrm{VIS}} + K_{\downarrow\mathrm{NIR}}] - \tau_{c,\odot,\mathrm{VIS}} K_{\downarrow\mathrm{VIS}}}{K_{\downarrow\mathrm{NIR}}} \tag{11}$$

where $\tau_{c,\odot}$ and $\tau_{c,\odot,\mathrm{VIS}}$ are calculated using $\kappa_{\odot}$ and $\kappa_{\odot,\mathrm{VIS}}$ respectively in equation (7).

Under cloudy skies, the hemispherical distribution of diffuse shortwave radiation is modelled using the generally accepted 'standard overcast' distribution (e.g. Steven and Unsworth, 1980), where the shortwave radiation $D(Z)$ emanating from a sky zenith angle Z is approximated as

$$D(Z) = D(0)\left[\frac{1 + 1{\cdot}23\cos Z}{1 + 1{\cdot}23}\right] \tag{12}$$

i.e. $D(0) = 2{\cdot}23D(90°)$. Equation (12) must be integrated over the sky hemisphere to obtain the cloudy-sky visible and total transmissivities $\tau_{c,\otimes,\mathrm{VIS}}$ and $\tau_{c,\otimes}$ respectively. A simple weighting calculation proposed by Goudriaan (1988) is used:

$$\tau_{c,\otimes} = 0{\cdot}308\tau_{c,\odot}(Z = 15°) + 0{\cdot}514\tau_{c,\odot}(Z = 45°) + 0{\cdot}178\tau_{c,\odot}(Z = 75°) \tag{13}$$

$$\tau_{c,\otimes,\mathrm{VIS}} = 0{\cdot}308\tau_{c,\odot,\mathrm{VIS}}(Z = 15°) + 0{\cdot}514\tau_{c,\odot,\mathrm{VIS}}(Z = 45°) + 0{\cdot}178\tau_{c,\odot,\mathrm{VIS}}(Z = 75°) \tag{14}$$

The cloudy-sky near-infrared transmissivity is again obtained as a residual, as in equation (11):

$$\tau_{c,\otimes,\mathrm{NIR}} = \frac{\tau_{c,\otimes}[K_{\downarrow\mathrm{VIS}} + K_{\downarrow\mathrm{NIR}}] - \tau_{c,\otimes,\mathrm{VIS}} K_{\downarrow\mathrm{VIS}}}{K_{\downarrow\mathrm{NIR}}} \tag{15}$$

Finally, the visible and total canopy transmissivities for partly cloudy skies are approximated using equations analogous to (6):

$$\tau_c = \frac{\tau_{c,\odot} K_{\downarrow D} + \tau_{c,\otimes} K_{\downarrow d}}{K_{\downarrow D} + K_{\downarrow d}} \tag{16}$$

$$\tau_{c,VIS} = \frac{\tau_{c,\odot,VIS} K_{\downarrow D} + \tau_{c,\otimes,VIS} K_{\downarrow d}}{K_{\downarrow D} + K_{\downarrow d}} \tag{17}$$

The near-infrared canopy transmissivity can then be obtained using an equation analogous to (11) and (15).

Having obtained the visible and near-infrared canopy albedos and transmissivities, the net shortwave radiation totals $K_{*,c}$ for the canopy and $K_{*,g/s}$ the underlying ground or snow cover can be calculated as:

$$K_{*,g/s} = \hat{\tau}_{c,VIS} K_{\downarrow VIS} [1 - \alpha_{g/s,VIS}] + \hat{\tau}_{c,NIR} K_{\downarrow NIR} [1 - \alpha_{g/s,NIR}] \tag{18}$$

$$K_{*,c} = K_{\downarrow VIS} [1 - \hat{\alpha}_{c,VIS}] + K_{\downarrow NIR} [1 - \hat{\alpha}_{c,NIR}] - K_{*,g/s} \tag{19}$$

where the carets denote 'composite canopy' values, calculated as weighted averages over the four major vegetation groups, and $\alpha_{g/s,VIS}$ and $\alpha_{g/s,NIR}$ are the soil or snow visible and near-infrared albedos respectively. Soil albedos are obtained from the all-wave ground albedo α_g (defined in equation (9) of Verseghy, 1991) by making use of the observation that for most soils, $\alpha_{g,NIR} \cong 2{\cdot}0\,\alpha_{g,VIS}$. Snow albedos are calculated as in equations (32) and (33) of Verseghy (1991), with visible albedos of 0·95, 0·84 and 0·61 and near-infrared albedos of 0·72, 0·56 and 0·38 as the boundary values for fresh snow, old dry snow and old melting snow respectively.

The net longwave radiation amounts absorbed by the canopy and the underlying surface, $L_{*,c}$ and $L_{*,g/s}$ respectively, are modelled more simply. A sky view factor χ, describing the degree of canopy closure, is defined as the fraction of sky that the ground underlying the canopy sees. According to studies reported in the literature, the following relations can be defined for the four main canopy types:

$$\chi = \exp(-0{\cdot}5\Lambda) \quad \text{(needleleaf trees)} \tag{20a}$$

$$\chi = \exp(-1{\cdot}5\Lambda) \quad \text{(broadleaf trees)} \tag{20b}$$

$$\chi = \exp(-0{\cdot}8\Lambda) \quad \text{(crops and grass)} \tag{20c}$$

Equations for $L_{*,c}$ and $L_{*,g/s}$ can therefore be written as:

$$L_{*,g} = (1 - \hat{\chi})\sigma \bar{T}_c^4 + \hat{\chi} L_{\downarrow} - \sigma T(0)^4 \tag{21}$$

$$L_{*,c} = (1 - \hat{\chi})(L_{\downarrow} + \sigma T(0)^4 - 2\sigma \bar{T}_c^4) \tag{22}$$

where $\hat{\chi}$ is the 'composite canopy' sky view factor averaged over the four major vegetation groups, $L_{\downarrow}$ is the incoming atmospheric longwave radiation, $\bar{T}_c$ is the effective canopy temperature and $T(0)$ is the temperature of the underlying ground. The canopy is modelled as behaving like a black body because the complex orientation of leaves in most vegetation stands can be assumed to lead to a high degree of radiation trapping and therefore to an effective emissivity of unity.

2.2. Sensible and latent heat fluxes

Energy fluxes from the canopy to the boundary layer are modelled using the bulk aerodynamic approach. The sensible heat flux from the canopy is written as

$$Q_{H,c} = \rho_a c_P (T_a - \bar{T}_c)/r_a \tag{23}$$

where ρ_a, c_P and T_a represent the density, specific heat and temperature respectively of the air above the vegetation, and r_a is the aerodynamic resistance. The latter is calculated from the surface drag coefficient C_D and the wind speed V_a above the canopy as

$$r_a = [C_D V_a]^{-1} \tag{24}$$

For a planar surface, the drag coefficient for heat and water vapour fluxes, $C_{D,E}$, can be taken to be equal to that for momentum, $C_{D,M}$. The expression for $C_{D,M}$ is

$$C_{D,M}=\left[\frac{k}{\ln(z_{ref}/z_{o,M})}\right]^2\Phi_M{}^2 \tag{25}$$

where z_{ref} is a reference height where $\delta V/\delta z\rightarrow 0$, $z_{o,M}$ is the surface roughness length for momentum transfer, and Φ_M is a stability correction factor dependent, among other things, on $z_{o,M}$ (see McFarlane *et al.*, 1992). However, in the case of rough surfaces such as those found in nature, the effective source height for sensible and latent heat transfers is not necessarily the same as that for momentum. In fact, it is found that while the roughness lengths for heat and water vapour transfer can be considered as approximately equal, this roughness length $z_{o,E}$ can be as much as an order of magnitude less than $z_{o,M}$. Following results presented by Garratt and Hicks (1973), Brutsaert (1979) and others, the following relations are used to obtain $z_{o,E}$ from $z_{o,M}$ for the four major vegetation types and for bare soil:

$$z_{o,E}=z_{o,M}/2{\cdot}0 \quad \text{(trees)} \tag{26a}$$

$$z_{o,E}=z_{o,M}/7{\cdot}0 \quad \text{(crops)} \tag{26b}$$

$$z_{o,E}=z_{o,M}/12{\cdot}0 \quad \text{(grass)} \tag{26c}$$

$$z_{o,E}=z_{o,M}/3{\cdot}0 \quad \text{(bare soil)} \tag{26d}$$

In addition to this, when the roughness elements are large, as in plant communities, the logarithmic wind profile is effectively shifted upward by a distance d, the so-called zero-plane displacement (assumed to be zero for bare soil). The parameters $z_{o,m}$ and d are calculated from the canopy height H using the simple relations $z_{o,M}=0{\cdot}10H$ and $d=0{\cdot}70H$. The composite canopy zero-plane displacement $\hat{d}$ is calculated, like the other composite canopy parameters, as a simple weighted linear average over the four major vegetation groups; the composite canopy roughness lengths $\hat{z}_{o,M}$ and $\hat{z}_{o,E}$, however, are determined using logarithmic averaging, as suggested by Taylor (1987). Thus, the equations for $C_{D,E}$ and $C_{D,M}$ become

$$C_{D,E}=\left[\frac{k}{\ln(z_{ref}-\hat{d})/\hat{z}_{o,E})}\right]\left[\frac{k}{\ln(z_{ref}-\hat{d})/\hat{z}_{o,M})}\right]\Phi_E\Phi_M \tag{27}$$

$$C_{D,M}=\left[\frac{k}{\ln(z_{ref}-\hat{d})/\hat{z}_{o,M})}\right]^2\Phi_M{}^2 \tag{28}$$

where Φ_E is the stability correction factor calculated using $\hat{z}_{o,E}$. At present, z_{ref} is assigned a constant value of 50 m.

Since the wind speed under the canopy can be assumed to be small, sensible heat transfer from the ground under the canopy is set equal to zero under stable conditions. Under unstable conditions, Townsend's (1964) equation for free convection is used, in a form derived from the analysis of Deardorff (1972):

$$Q_{H,g/s}=1{\cdot}9\times 10^{-3}\rho_a c_P[T_{a,c}-T(0)][T'(0)-T'_{a,c}]^{1/3} \tag{29}$$

where $T(0)$ and $T_{a,c}$ are the actual and $T'(0)$ and $T'_{a,c}$ are the virtual temperatures of the ground surface under the canopy and of the air within the canopy respectively. The virtual temperatures are calculated as

$$T'(0)=T(0)[1{\cdot}0+0{\cdot}61q(0)] \tag{30}$$

$$T'_{a,c}=T_{a,c}[1{\cdot}0+0{\cdot}61q_{a,c}] \tag{31}$$

The specific humidity of air at a soil surface, $q(0)$, is given by equation (13) in Verseghy (1991); for a snow surface, $q(0)$ is equal to the saturation specific humidity at $T(0)$. The temperature of the air within the canopy is taken to be equal to $\bar{T}_c$, and the specific humidity is assumed to be equal to that of the air above the canopy. (Deardorff (1978) calculates $T_{a,c}$ and $q_{a,c}$ as linear combinations of the values for the canopy, the

ground below it and the air above it, but remarks that the calculation is not sensitive to the magnitudes of the three weighting factors.)

The latent heat flux from the canopy is calculated using an equation analogous to that for sensible heat. If the canopy surfaces are covered with a film of intercepted precipitation (or if the vapour flux is toward the canopy), evaporation (sublimation) takes place at the potential rate:

$$Q_{E,c,wet}=\frac{L_v\rho_a[q_a-q_{sat}(\bar{T}_c)]}{r_a} \tag{32}$$

where L_v is the latent heat of vaporization of water and $q_{sat}(\bar{T}_c)$ is the saturation specific humidity at $\bar{T}_c$. If the canopy is dry, a resistance r_c must be incorporated into the denominator of (32), to account for the bulk stomatal resistance of the canopy leaves to transpiration:

$$Q_{E,c,dry}=\frac{L_v\rho_a[q_a-q_{sat}(\bar{T}_c)]}{r_a+r_c} \tag{33}$$

Dense, green, unstressed canopies are generally found to have similar, low values of stomatal resistance, ranging from 25 to 100 s m^{-1}. A reasonable representative value for this minimum resistance $r_{c,min}$ is 50 s m^{-1} (Sherratt and Wheater, 1984). If the canopy is incomplete or immature, the resistance is greater. Making use of the assumption that leaf resistances act in parallel, i.e. $1/r_c(\Lambda)=\Lambda/r_l$, where r_l is the stomatal resistance of a single leaf, it can readily be deduced that if $\Lambda<\Lambda_{max}$ for a given canopy type, its unstressed canopy resistance can be obtained as

$$r_c(\Lambda)=r_{c,min}[\Lambda_{max}/\Lambda] \tag{34}$$

Various environmental factors may act upon the canopy to produce stress and cause the stomata to close to prevent excessive transpiration, thus leading to an increase in r_c. The most important of these factors are the incoming solar radiation $K_\downarrow$, the air vapour pressure deficit Δe, the leaf water potential ψ_l, and the canopy temperature $\bar{T}_c$. Most researchers assume the effects of these to be multiplicative. Variations in ψ_l are difficult to model, as they depend on poorly understood aspects of plant physiology; therefore, like many other models, CLASS uses the soil moisture suction $\psi_{s,r}$ in the rooting zone as a surrogate for ψ_l (since the former is in fact the most important factor influencing the latter). Also, to avoid the risk of runaway feedback effects, T_a is used in the calculation of r_c as a surrogate for $\bar{T}_c$. Thus,

$$r_c=\hat{r}_c f_1(K_\downarrow)f_2(\Delta e)f_3(\psi_{s,r})f_4(T_a) \tag{35}$$

where $\hat{r}_c$ is the composite canopy value, averaged over the four major vegetation groups, of the unstressed canopy resistance calculated using equation (34). No data set exists that reports the simultaneous variation of r_c with respect to all of the above parameters, even for one vegetation type. There is also little agreement as to what form the functional dependence should take (e.g. Federer, 1979; Avissar *et al*, 1985; Simpson *et al.*, 1985; Stewart, 1988). This is still an area of ongoing research in the continuing development of CLASS. At present, the following simple relations are used:

$$f_1(K_\downarrow)=\max(1{\cdot}0,\ 500{\cdot}0/K_\downarrow-1{\cdot}5) \qquad (K_\downarrow \text{ in W m}^{-2}) \tag{36a}$$

$$f_2(\Delta e)=\max(1{\cdot}0,\ \Delta e/5{\cdot}0) \qquad (\Delta e \text{ in mbar}) \tag{36b}$$

$$f_3(\psi_{s,r})=\max(1{\cdot}0,\ \psi_{s,r}/40{\cdot}0) \qquad (\psi_{s,r} \text{ in m}) \tag{36c}$$

$$\left.\begin{aligned} f_4(T_a)&=1{\cdot}0, && 40^\circ\text{C}>T_a>0^\circ\text{C}\\ &=5000{\cdot}0/\hat{r}_c, && T_a\geqslant 40^\circ\text{C or } T_a\leqslant 0^\circ\text{C}\end{aligned}\right\} \tag{36d}$$

The value used for $\psi_{s,r}$ is the minimum value of soil moisture suction found for the soil layers contained within the rooting zone; this follows the approach of Radcliffe *et al.* (1980), who assume that plants optimize their energy expenditures by extracting water preferentially from the soil layer with the lowest energy level.

Given the evaporation rates from the wet and dry fractions of the canopy, the total evaporation rate $Q_{E,c}$ can be calculated. The wet portion of the canopy is divided into the fractions covered by liquid water, X_l, and by snow or ice, X_s. These are simply defined as

$$X_l = W_l/W_{max}; \qquad X_s = W_s/W_{max} \tag{37}$$

where W_l and W_s represent the masses of rain and snow or ice respectively that are stored on the canopy, and W_{max} is the canopy storage capacity in kg m^{-2} (see section 2.3 below). (A simple linear relation of this sort has been found by Hancock and Crowther (1979) to provide a more realistic parameterization of canopy wetness than the more complex form $X_l=(W_l/W_{max})^{2/3}$ proposed by Deardorff (1978).) If $X_s>0$, transpiration cannot be occurring from the dry portion of the canopy, since $\bar{T}_c$ must be $\leqslant 0°C$ and the stomata are therefore closed. In this case,

$$Q_{E,c} = \frac{[X_l L_v + X_s L_s]\rho_a[q_a - q_{sat}(\bar{T}_c)]}{r_a} \qquad (\bar{T}_c \leqslant 0°C) \tag{38}$$

where L_s is the latent heat of sublimation. If $X_s=0$, on the other hand, transpiration may be occurring, but the correction for L_s is not required; thus,

$$Q_{E,c} = L_v\rho_a(q_a - q_{sat}(\bar{T}_c))\left[\frac{X_l}{r_a} + \frac{(1-X_l)}{r_a+r_c}\right] \qquad (\bar{T}_c > 0°C) \tag{39}$$

Finally, for evaporation from the ground surface under the canopy, the same strategy is used as that for sensible heat transfer. Under stable conditions, $Q_{E,g/s}$ is set equal to zero; under unstable conditions, an equation analogous to (29) is used:

$$Q_{E,g/s} = 1{\cdot}9\times 10^{-3} L_v\rho_a[q_{a,c} - q(0)][T'(0) - T'_{a,c}]^{1/3} \tag{40}$$

2.3. Moisture storage on the canopy

Precipitation arriving at the vegetation tops is either intercepted by the foliage, or falls through gaps in the canopy to the ground. Making use of the sky view factor $\hat{\chi}$ defined above, the precipitation rate at the ground surface and the rate of interception by the canopy are calculated as $\hat{\chi}r$ and $(1-\hat{\chi})r$ respectively, where r is the incoming precipitation rate. The maximum amount of rain or snow that can be stored on vegetation surfaces, W_{max}, strictly speaking depends on a number of factors such as precipitation intensity, wind speed, canopy architecture, etc., and therefore varies with both vegetation type and precipitation event. However, field observations reported in the literature indicate that the following simple, averaged relationship works well for both rain and snow and for a wide variety of vegetation types and precipitation events:

$$W_{max} = 0{\cdot}20\Lambda \qquad (\text{kg m}^{-2}) \tag{41}$$

In reality, W_{max} refers to the canopy storage capacity after drainage has ceased. During major storms, it is found that W_{max} is often temporarily exceeded (e.g. Rutter *et al.*, 1971). However, it generally can be assumed that the excess water drains away fairly quickly (i.e. within 30 minutes; cf. Gash, 1979). A study by Mahfouf and Jacquemin (1989) has in fact shown that using a simple model of the type described above leads to a negligible loss of accuracy in calculating $Q_{E,c}$ when tested against HAPEX data and compared with the results of a much more complex model incorporating drainage from the canopy. Thus, in CLASS, interception of precipitation by foliage proceeds until W_{max} is reached; after this point, any excess is added to the precipitation reaching the ground.

The evapotranspiration flux from the canopy is assumed for the sake of simplicity to deplete the stored moisture first, since the associated resistance is less. The evaporation rates E_l and E_s of the liquid and frozen moisture stored on the canopy are calculated as

$$E_l = \frac{Q_{E,c}X_l}{L_vX_l + L_sX_s} \tag{42}$$

$$E_s = \frac{Q_{E,c} X_s}{L_v X_1 + L_s X_s} \tag{43}$$

When the moisture stored on the canopy has been exhausted, transpired water is removed from the soil. The rate of water extraction from each soil layer i in the rooting zone, $E_{T,i}$, is calculated using a weighting function $F_{r,i}$ defined on the basis of the fractional volume of roots R_i and the soil moisture suction $\psi_{s,i}$ in that layer:

$$F_{r,i} = \frac{R_i[\psi_{max} - \psi_i]}{\sum_{i=1}^{N} R_i[\psi_{max} - \psi_i]} \tag{44}$$

where $\psi_i = \min(\psi_{max}, \psi_{s,i})$, ψ_{max} is the critical soil moisture suction at which transpiration effectively ceases (taken to be 150 m), and N is the number of soil layers in the rooting zone. To obtain R_i, a function $R(z)$ is defined as the fractional root volume below a given depth z. The consensus in the literature is that $R(z)$ is usually exponential in form:

$$R(z) = a_1 e^{-a_2 z} + a_3 \tag{45}$$

where a_1, a_2, and a_3 are constants. According to Feddes *et al.* (1974), for many varieties of crops, grasses and trees, $a_2 \cong 3{\cdot}0$. Making use of the boundary conditions $R(0)=1$ and $R(\hat{z}_r)=0$, where $\hat{z}_r$ is the averaged, composite canopy rooting depth, equation (45) becomes

$$R(z) = \frac{\exp(-3{\cdot}0z) - \exp(-3{\cdot}0\hat{z}_r)}{1 - \exp(-3{\cdot}0\hat{z}_r)} \tag{46}$$

R_i is then calculated from $R(z)$ as

$$R_i = R(z_{i-1}) - R(z_i) \tag{47}$$

where z_{i-1} and z_i are the depths of the top and bottom of the soil layer respectively (see Figure 1 in Verseghy, 1991). Finally, $E_{T,i}$ can be calculated (in m^3 water per m^3 soil) as:

$$E_{T,i} = \frac{Q_{E,c} F_{r,i}}{\rho_w L_v \Delta z_i} \tag{48}$$

where ρ_w is the density of water and Δz_i is the thickness of the soil layer.

2.4. Canopy and ground temperatures

The canopy and ground surface temperatures are calculated by iterative solution of the respective energy balance equations, which are expressed as non-linear functions of $\bar{T}_c$ and $T(0)$ alone. The energy balance equations for the surface under the canopy and for the canopy itself are written as

$$K_{*,g/s} + L_{*,g/s} + Q_{H,g/s} + Q_{E,g/s} = G_o \tag{49}$$

$$K_{*,c} + L_{*,c} + Q_{H,c} - Q_{H,g/s} + Q_{E,c} + S_c = \frac{C_c}{\Delta t}[\bar{T}_c(t) - \bar{T}_c(t-1)] \tag{50}$$

All of the variables on the left-hand sides have been defined in the above sections except for two: S_c is a source (or sink) term for freezing or thawing of moisture stored on the canopy, re-evaluated within each iteration, and G_o is the heat flux into the ground, obtained from equation (16) in Verseghy (1991). The variable C_c represents the heat capacity of the canopy in J m^{-2} K^{-1}, and is calculated as

$$C_c = c_c \hat{W}_c + c_w W_1 + c_s W_s \tag{51}$$

where the c terms are the specific heats of vegetation, water and snow respectively, and $\hat{W}_c$ is the standing mass of the composite canopy. The variable c_c is assigned a value of $2{\cdot}7 \times 10^3$ J kg^{-1} K^{-1}, and $\hat{W}_c$ is

calculated by weighted averaging over the four major canopy groups. (C_c is determined separately for the below 0°C and above 0°C limbs of the calculation for S_c.)

It is assumed in equation (50) that heated air rising from the ground below the vegetation cannot pass through the canopy without warming it; $Q_{H,g/s}$ is therefore considered as a heat source for the canopy. Water vapour rising from the ground, however, is assumed to pass through the canopy without condensing on the foliage, since the foliage is assumed to be at the same temperature as the intracanopy air (see section 2.2 above). In effect, $Q_{H,g/s}$ and $Q_{E,g/s}$ are treated as corrections to the classic, bulk micrometeorological treatment of the canopy developed and refined by Monteith (1965), Thom and Oliver (1977), and others.

Strictly speaking, the canopy and ground surface temperatures, $\bar{T}_c$ and $T(0)$, should be solved for simultaneously. However, in order to avoid the complexity of solving a pair of highly non-linear equations in two unknowns, $T(0)$ is obtained first using the canopy temperature from the previous time step, and $\bar{T}_c$ is then calculated using this value. (This can be theoretically justified by noting that the temperature of the underside of the canopy will in fact be damped, and will experience some slight time lag with respect to $\bar{T}_c(t)$.) In order to ensure that energy is conserved, the heat flux into the ground is subsequently recalculated using the new value of $\bar{T}_c$.

Finally, from the foregoing discussion the reflected shortwave, emitted longwave, sensible and latent heat fluxes of the canopy covered land surface, as seen by the overlying atmosphere, can be written respectively as

$$K^{\uparrow} = \hat{\alpha}_c K_{\downarrow} \tag{52}$$

$$L^{\uparrow} = (1-\hat{\chi})\sigma \bar{T}_c^4 + \hat{\chi}\sigma T(0)^4 \tag{53}$$

$$Q_H = -Q_{H,c} \tag{54}$$

$$Q_E = -Q_{E,c} - Q_{E,g/s} \tag{55}$$

2.5. Seasonal variations in canopy parameters

To account for seasonal variations in the morphological characteristics of the four major canopy types, a growth index γ is carried for each. This has a value of 1 during periods when the vegetation is mature and/or fully leafed, and a value of 0 during dormant and leafless periods; the transition between the two is taken to be linear. For trees, the onset of the transition period is assumed to be triggered by changes in the air temperature T_a and the temperature of the top soil layer $\bar{T}_{g,1}$. The transition to dormancy begins when T_a first falls below 0°C. Breaking of dormancy occurs when both T_a and $\bar{T}_{g,1}$ rise above 0°C; if either drops back below 0°C after this point, γ for the trees is set back to 0. For needleleaf trees, the transition periods each last for 2 months; for broadleaf trees, they last for 1 month. For the growth index of crops, the Earth is divided into 10° latitude bands. Within each band and for each hemisphere, the beginning of crop growth and the end of harvest are specified as occurring on certain days of the year. Following information gleaned from the literature, it is assumed that crops take 2 months to reach maturity, and that 1 month elapses between the time that senescence begins and the time that harvest is over. Finally, grass is assigned a growth index of 1 throughout the year, since its annual variations in height and leaf area index can be considered as negligible.

The roughness length for momentum at vegetation maturity, $z_{o,max}$, is carried for all four major vegetation classes for each grid square. Thus, at every time step the maximum height of each vegetation class, H_{max}, can be calculated as $H_{max} = 10{\cdot}0 z_{o,max}$ (see the discussion following equation (26) above). The height of trees does not undergo any seasonal variation, and thus is always equal to H_{max}. The height of crops or grass, however, may fall below H_{max} due to immature growth stage (in crops) or to partial burying by snow. Thus, the height of vegetation for the four major vegetation groups is calculated at each time step as

$$H = H_{max} \quad \text{(trees)} \tag{56a}$$

$$H = \gamma H_{max} - z_s \quad \text{(crops)} \tag{56b}$$

$$H = H_{max} - z_s \quad \text{(grass)} \tag{56c}$$

where z_s is the snow depth. The values of $z_{o,M}$ and d are recalculated at each time step from the current values of H.

The standing mass W_c of each of the four canopy groups is assigned a maximum value for each grid square. For trees, W_c is always equal to $W_{c,max}$; leaf fall is assumed to cause a negligible change in canopy mass. For crops and grass, W_c is modified, making use of the instantaneous value of H, to account for growth stage and the burying of vegetation by snow:

$$W_c = W_{c,max} \qquad \text{(trees)} \tag{57a}$$

$$W_c = W_{c,max} H/H_{max} \qquad \text{(crops and grass)} \tag{57b}$$

The vegetation rooting depth z_r is not affected by snow cover, and therefore remains at its maximum value for trees and grass over each grid square. For crops, it is corrected for growth stage:

$$z_r = z_{r,max} \qquad \text{(trees and grass)} \tag{58a}$$

$$z_r = \gamma z_{r,max} \qquad \text{(crops)} \tag{58b}$$

Leaf area index varies seasonally between maximum and minimum values, determined separately for each vegetation type. As in the above calculations, the presence of snow cover does not affect the calculated value of Λ for trees; a correction similar to that for the calculation of W_c is made for crops and grass. (It is assumed for the latter two vegetation types that leaves are distributed approximately uniformly with height.) Thus,

$$\Lambda = \Lambda_{min} + \gamma[\Lambda_{max} - \Lambda_{min}] \qquad \text{(trees)} \tag{59a}$$

$$\Lambda = H/H_{max}[\Lambda_{min} + \gamma[\Lambda_{max} - \Lambda_{min}]] \qquad \text{(crops and grass)} \tag{59b}$$

Finally, each of the four canopy types is assigned a maximum fractional areal coverage $X_{c,max}$ for each grid square. For trees, the fractional cover X_c at any given time step is taken as equal to $X_{c,max}$. For crops and grass, the effective canopy cover is assumed to be decreased whenever the leaf area index is calculated as falling below 1. In such cases X_c is recalculated as $X_{c,max}\Lambda$, Λ is set back to 1, and an amount $X_{c,max} - X_c$ is added to either the snow-covered or to the bare-soil fraction of the grid square, depending on whether snow cover is present under the canopy or not.

2.6. Implementation in the Canadian Climate Centre GCM

Global data on certain vegetation parameters are required in order to run CLASS in a GCM. From the above discussion, it can be seen that the variables required for each grid square are $\bar{\alpha}_{c,VIS}$, $\bar{\alpha}_{c,NIR}$, $z_{o,max}$, Λ_{max}, Λ_{min}, $W_{c,max}$, $z_{r,max}$, and $X_{c,max}$ for the four major vegetation groups. This information is obtained by making use of the global archive of Wilson and Henderson-Sellers (1985), which contains listings of primary and secondary land covers at a resolution of $1° \times 1°$. Following a suggestion made in their paper, the 51 land cover types recognized by them are assumed to be characterizable by varying percentages of 24 major categories: e.g. tropical broadleaf tree, long grass, bare soil, glacier ice, etc. On the basis of this information, and assigning a weighting of 75 per cent and 25 per cent to the primary and secondary land cover types respectively, the 24 major categories are obtained at the required GCM grid resolution by performing a weighted average calculation over all of the $1° \times 1°$ squares or parts thereof that fall within each grid square.

If ocean is found to cover more than half of a given grid square, it is assumed to be ocean; if more than half is covered by glacier ice, it is considered as glacier ice. (The latter is treated in effect like bare soil with a possible snow cover, as outlined in Verseghy (1991): the volume fraction of frozen water in the three 'soil' layers is taken to be 1, the thermal properties of ice are used for each layer, and no infiltration of water is allowed at the surface.) To each of the remaining land cover categories, CLASS assigns characteristic values of $X_{c,max}$, $\bar{\alpha}_{c,VIS}$, $\bar{\alpha}_{c,NIR}$, $z_{o,max}$, Λ_{max}, Λ_{min}, $W_{c,max}$, and $z_{r,max}$ (the latter four for vegetation classes only), obtained from the literature. Each land cover category is then assigned to one of five major groups: bare soil, needleleaf trees, broadleaf trees, crops, and grass. (Urban areas are classified as bare soil at present, and are

considered as modifying the albedo and roughness length of bare soil according to their fractional coverage of the grid square.) The canopy parameters for each of the four major vegetation types are then calculated as weighted averages over the land cover categories present on the grid square that fall into that group. Linear averaging is done for all of the variables except for $z_{o,max}$; following Taylor (1987), this is calculated as a logarithmic average. The parameters associated with each of the 24 land cover categories are listed in Table I.

Global data sets of soil properties are also required. The work of Wilson and Henderson-Sellers is again used to obtain the basic information necessary to evaluate these parameters. The latter provide global data sets, at a resolution of $1° \times 1°$, of qualitative evaluations of soil colour (light, medium, dark), texture (fine, medium, coarse), and drainage (free, impeded, clear). The three soil colour categories are assigned wet and dry albedo values taken from table IX in their paper. The three soil textural categories are assigned fractional contents of sand and clay, corresponding to those associated with representative clay, loam, and sandy soils respectively in the standard USDA texture triangle. The three drainage categories are assigned rough values of ξ, a crude 'drainage efficiency' coefficient, of 1·0, 0·5, and 0·0 respectively. The average values of the wet and dry soil albedos, the sand and clay fractions in the soil, and the drainage efficiency coefficient, are then calculated as weighted averages over the $1° \times 1°$ squares that occur within each grid square. From the fractional sand and clay contents of the soil, the values of the texture-dependent parameters ϑ_p, b, ψ_{sat}, K_{sat}, etc. (see Verseghy, 1991) can be calculated. As a rough quantification of the effects of drainage impedance over the grid square, the calculated drainage rate at the bottom of the soil profile is multiplied by ξ.

At the beginning of a GCM run, the vegetation and soil parameters are calculated as described above for the required resolution. At the beginning of each time step, the temperatures of the canopy, snow, and soil layers, the liquid and frozen moisture stored on the canopy and in the soil layers, the snow albedo, density, and mass, and the growth index are retrieved from memory. Each grid square is then divided up into a maximum of four subareas: vegetation over snow; vegetation over soil; snow cover; and bare ground. The

Table I. Parameters associated with land cover categories used in CLASS

	Code[a]	$\bar{\alpha}_{c,VIS}$	$\bar{\alpha}_{c,NIR}$	$z_{o,max}$ (m)	Λ_{max}	Λ_{min}	$W_{c,max}$ (kg m^{-2})	$z_{r,max}$ (m)
Evergreen needleleaf tree	1	0·03	0·19	1·5	5·0	4·0	25·0	1·0
Evergreen broadleaf tree	2	0·03	0·23	3·5	10·0	10·0	50·0	0·2
Deciduous needleleaf tree	1	0·03	0·19	1·0	4·0	0·5	15·0	1·0
Deciduous broadleaf tree	2	0·05	0·29	2·0	6·0	0·5	20·0	2·0
Tropical broadleaf tree	2	0·03	0·23	3·0	10·0	10·0	40·0	5·0
Drought deciduous tree	2	0·05	0·29	0·8	4·0	4·0	15·0	5·0
Evergreen broadleaf shrub	2	0·04	0·28	0·15	4·0	4·0	8·0	5·0
Deciduous shrub	2	0·05	0·29	0·15	4·0	0·5	8·0	1·0
Thorn shrub	2	0·06	0·32	0·15	3·0	3·0	8·0	5·0
Short grass and forbs	4	0·06	0·34	0·02	3·0	3·0	1·5	1·2
Long grass	4	0·05	0·31	0·08	4·0	4·0	3·0	1·2
Arable	3	0·06	0·34	0·08	4·0	0·0	2·0	1·2
Rice	3	0·06	0·36	0·08	6·5	0·0	2·0	1·2
Sugar	3	0·05	0·31	0·35	5·0	0·0	5·0	1·0
Maize	3	0·05	0·31	0·25	4·0	0·0	5·0	1·5
Cotton	3	0·07	0·43	0·10	5·0	0·0	2·0	2·0
Irrigated crop	3	0·06	0·36	0·08	4·0	0·0	2·0	5·0
Urban	–	0·09	0·15	1·35	–	–	–	–
Tundra	4	0·05	0·29	0·01	1·5	1·5	0·2	0·1
Swamp	4	0·03	0·25	0·05	1·5	1·5	1·0	5·0
Bare soil	–	See text		0·0005	–	–	–	–
Glacier ice	–	See text		0·002	–	–	–	–

[a] Vegetation type to which each land cover is assigned: 1 = needleleaf tree, 2 = broadleaf tree, 3 = crops, 4 = grass.

total fractional snow cover X_s is obtained from equation (35) in Verseghy (1991); the total canopy cover $X_{c,tot}$ is calculated as the sum of the X_c values for the four major canopy types. From these two parameters, the fractional grid square coverages of the four subareas listed above are calculated as $X_{c,tot}X_s$, $X_{c,tot}(1-X_s)$, $(1-X_{c,tot})X_s$, and $(1-X_{c,tot})(1-X_s)$ respectively. The current values of snow albedo and bare soil albedo are determined, and the composite canopy parameters are calculated separately for the canopy covered and canopy-and-snow covered subareas. For each of the four subareas, the energy and moisture fluxes at the canopy, at the ground surface, and between the soil layers are evaluated, the canopy, snow, and soil layer temperatures are updated, and the changes in liquid and frozen moisture stored on the canopy and ground surface and in the soil layers are calculated. Finally, the grid-square average values of the prognostic variables are calculated and stored back into memory.

3. MODEL TESTING AND COMPARISON WITH PREVIOUS SCHEME

Climate simulations were done using two versions of CLASS, in coupled mode with the Canadian Climate Centre (CCC) GCM. In the first version, ponded water remaining on the surface of grid squares at the end of each time step was carried over to the next time step, as described in Verseghy (1991). In the second version, any ponded water that had not infiltrated or evaporated by the end of a given time step was considered to be surface runoff, and was discarded. (This approximates the standard treatment given to ponded water in other GCMs.) These two runs were done in parallel with another one, which featured the old land surface scheme previously used in the GCM (McFarlane *et al.*, 1992). The bare soil model associated with the latter scheme is outlined in Verseghy (1991); where vegetation is present, a few simple modifications are made. For each grid square, the fractional coverage by bare soil, X_g, and the primary and secondary vegetation categories are specified from the data archive of Wilson and Henderson-Sellers (1985). To each of these vegetation categories are assigned characteristic values of visible and near-infrared albedo, snow masking depth, rooting depth, and the 'water use efficiency' parameter; grid-square average values of these terms are calculated by arbitrarily assigning weights of 0·67 and 0·33 to the primary and secondary vegetation categories respectively. The grid-square average albedo is calculated from equation (47) in Verseghy (1991), with α_g replaced by $[X_g\alpha_g+(1-X_g)\alpha_c]$, where α_c is the canopy albedo. The rooting depth is taken as specifying the depth of the 'bucket', and the water use efficiency parameter is incorporated into the calculation of the evaporation efficiency term β (equations (41) and (42) in Verseghy, 1991).

The three runs were all done using the same version of the CCC GCM. This was basically the model described in McFarlane *et al.* (1992), with the addition of some modifications made by Zhang and McFarlane to the parameterization of convection (paper in preparation). A model resolution of T32 was used, with 20 levels in the vertical. FGGE data for 1 January were used to initialize the runs; sea surface temperatures and sea ice extents were prescribed from observations. Each run was integrated for 14 months. Diagnostics were then calculated for the June–July–August season and for the following December–January–February season. In the discussion below, particular attention will be paid to the fields of seasonally averaged screen air temperature and precipitation.

3.1. Results for the June–July–August season

Global observed and modelled average values of screen temperature and precipitation for June, July, and August are presented in Table II. The values of the fields averaged over land surfaces alone are also provided; since sea surface temperatures are prescribed, these give a somewhat clearer picture of the performance of the models. From the information in the table, it can be seen that the old land surface scheme generates a climate that is on the whole too cool and too wet. When land surfaces only are considered, the globally averaged screen temperature is underestimated by 2·7°C, and the global precipitation rate is overestimated by 1·0 mm day^{-1}. The two versions of CLASS, on the other hand, generate climates that are too warm and too wet, but the anomalies are much smaller: 0·2–0·6°C and 0·6–0·7 mm day^{-1} respectively. The climate of the version that retains ponded water is slightly cooler and wetter than that of the version that discards it, because the greater amount of water available at the surface leads to higher evaporation rates.

Global plots of screen temperature anomalies (modelled–observed) are presented in Figure 1. Looking at the plot for the old scheme, it can be seen that cold temperatures are indeed widespread; negative anomalies are observed almost everywhere over land. This bias is probably caused mainly by the model's neglect of vegetation stomatal resistance to transpiration; Warrilow *et al.* (1986) and Sato *et al.* (1989) noted improvements in simulations of surface screen temperature and evaporation rates when land surface schemes incorporating this term were adopted. The only significant positive anomalies that are found occur over Greenland, the south-western USA, north-eastern Africa and the Middle East to northern India. However, positive anomalies also turn up in the same places in the plots for the two versions of CLASS, which suggests that the cause is not directly related to the formulation of the land surface scheme. In this case, it appears that the high temperatures are caused by incomplete information on the characteristics of the indigenous vegetation. In all of the above cases except Greenland, the anomalies occur over desert or semi-desert areas (the Köppen 'hot steppe' classification), which are described by Wilson and Henderson-Sellers (1985) as having a primary land cover of bare soil and a secondary land cover of thorn shrub. Hardly any data are available on the morphological characteristics of the latter vegetation type, and on the fluctuations in its

Table II. Global average values of surface fields: June–July–August

	Whole globe		Land only	
	Screen temperature (°C)	Precipitation rate (mm day^{-1})	Screen temperature (°C)	Precipitation rate (mm day^{-1})
Observed	15·9	2·9	13·8	2·4
CLASS—ponded water retained	16·1	2·9	14·0	3·1
CLASS—ponded water discarded	16·2	2·9	14·4	3·0
Old scheme	15·1	3·1	11·1	3·4

Figure 1. Global screen temperature (°C) anomaly plots (modelled–observed) for the June–July–August season. Diagonal shading indicates values greater than 4°C and cross- hatching values less than −4°C. Contour interval is 2°C; dashed contours indicate negative values. Observed fields were supplied by NCAR. (a) CLASS: ponded water retained; (b) CLASS: ponded water discarded; (c) old scheme

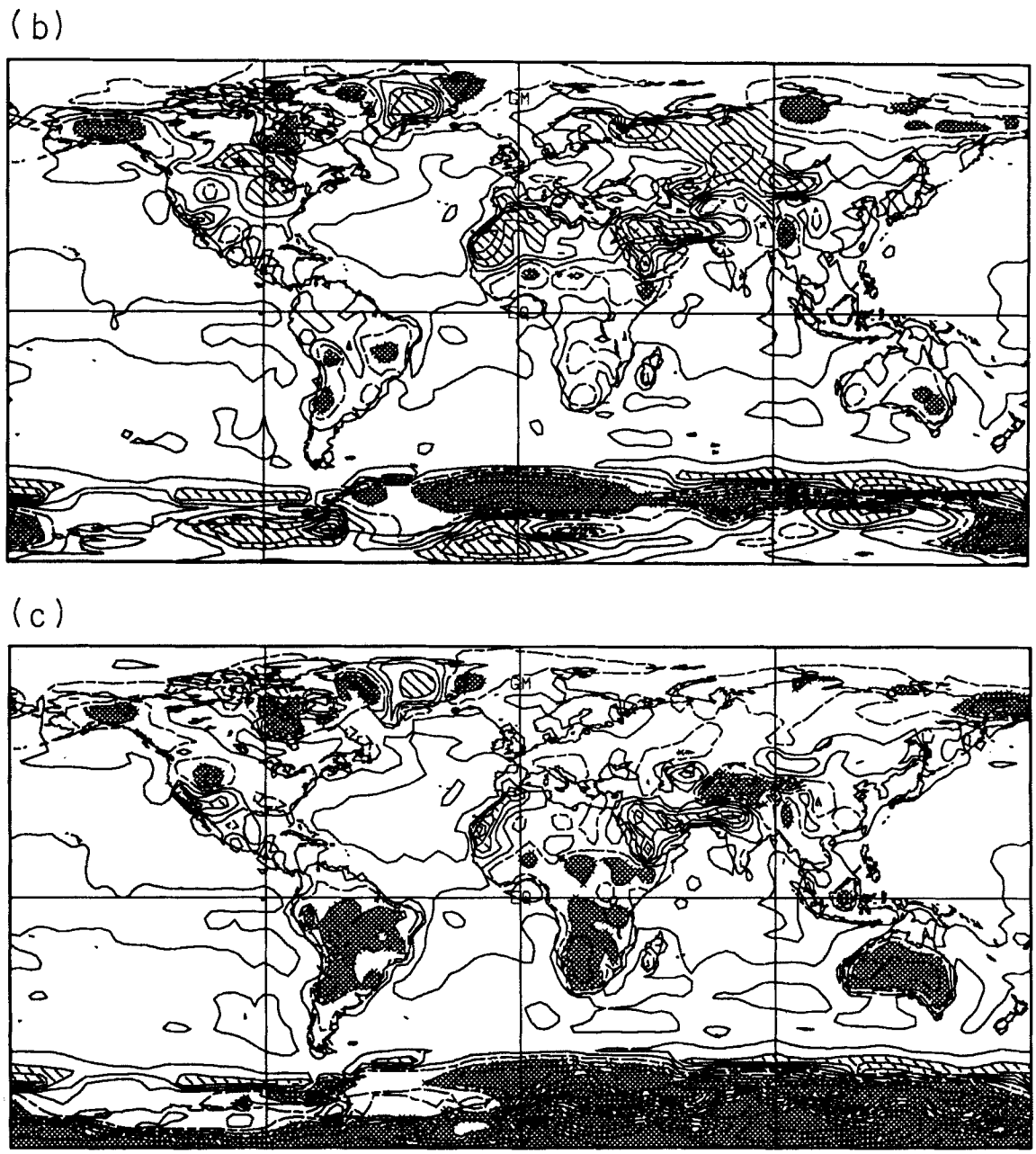

Figure 1. (Continued)

albedo and leaf area index between the dry and wet seasons; such variations are consequently neglected in both CLASS and the old model. The albedo of well-watered vegetation is typically considerably less than that of bare, sandy soil; it is therefore possible that the effective albedo of these areas is being underestimated during the dry season (Northern Hemisphere summer) and overestimated during the wet season. This hypothesis is borne out by the fact that these same areas experience negative screen temperature anomalies in December–January–February (Figure 4).

Another factor that may be contributing to the temperature anomalies observed over deserts in the old scheme is the use of the force-restore method to model the soil thermal regime. This method was developed to

handle diurnally periodic surface forcing, and therefore contains no mechanism corresponding to that provided by multiple soil layers to dampen long-term forcing (see Verseghy, 1991). Thus, surface temperatures over deserts, where the forcing is strongest, can be expected to be overestimated in summer and underestimated in winter. This hypothesis is supported by the fact that the anomalies over Northern Hemisphere deserts are positive, whereas those over Southern Hemisphere deserts, such as the Kalahari and central Australian, are negative. Further support is given by the fact that in December–January–February (Figure 4), this pattern is largely reversed: substantial negative anomalies are observed over the Sahara, Saudi Arabia, and south-eastern North America.

The runs done using CLASS show a more balanced pattern of positive and negative screen temperature anomalies. For the version with ponded water retained, sizeable anomalies of magnitudes greater than 4°C are only found in central Asia (outside of the areas mentioned above). This anomaly is possibly related to some flaw in the stomatal resistance formulation, which as pointed out above is quite crude. Comparing this plot to the one in which ponded water was discarded, it can be seen that the positive anomalies are greatly increased in area in the latter, particularly in central and north-western Asia and central North America. It would therefore seem that the assumption made in almost all GCMs, i.e. that excess surface water immediately becomes runoff, can lead to a surface soil moisture deficit in continental centres and consequently to substantial positive anomalies in surface screen temperature. In the old scheme, this effect is fortuitously obliterated by its strong tendency toward underestimation of screen temperatures.

The global precipitation anomaly plot for GCM runs done at a resolution of T32 tends to be somewhat chaotic in appearance, owing to the fact that at such low resolutions coastal and orographic precipitation patterns tend to be rather poorly reproduced. Zonal average plots of precipitation are therefore presented instead, for the three model versions compared with observations (Figure 2). Over the Northern Hemisphere, where land masses are large and the main source for continental precipitation is local evaporation, it can be seen that the high evaporation rates generated by the old scheme produce precipitation rates that are considerably overestimated, particularly between 40° and 65°N. Large local evaporation rates also lead to a sizeable positive anomaly at the ITCZ. In the Southern Hemisphere, on the other hand, where land areas are smaller and convergence of moisture from the oceans is a more important source of local precipitation, the cold anomaly over land masses seems to lead to decreased convergence, and thus to a more severe negative precipitation anomaly than is found in either version of CLASS.

Finally, plots of zonally averaged mean sea-level pressures for the three model versions are presented in Figure 3. It can be seen that both versions of CLASS perform substantially better than the old scheme, except in northern high latitudes. The low pressures generated by CLASS in this region can be traced mainly to the large positive screen temperature anomaly found over central Asia. It should be noted, however, that the seemingly more realistic pressures produced by the old scheme in northern high latitudes are associated with negative screen temperature anomalies. Unrealistically large areal extents for the subtropical highs in both hemispheres in the old scheme can also be traced to the low screen temperatures, which cause encroachment of the highs over land masses. Over Antarctica, on the other hand, pressures are underestimated by almost 10 hpa. This is caused by the fact that cold air draining off the continent onto relatively warm water sets up enhanced baroclinic conditions, which in turn lead to deepened subpolar lows.

3.2. Results for the December–January–February season

Table III lists global observed and modelled values of screen temperature and precipitation, averaged over the months of December, January and February, for the whole Earth and for land surfaces only. Again, it can be seen that the old scheme produces a climate that is too cold and too wet. Over land surfaces, the magnitude of the screen temperature anomaly is 3·0°C, and that of the precipitation anomaly is 0·9 mm day^{-1}. Both versions of CLASS are slightly too cold (by 0·3–0·4°C) and too wet (by 0·6–0·7 mm day^{-1}) over land; the version that discards water ponded on the surface is again marginally warmer and drier than that which retains it. This time, the former version comes closer to observations than the latter; the reason for this will become apparent from the discussion below.

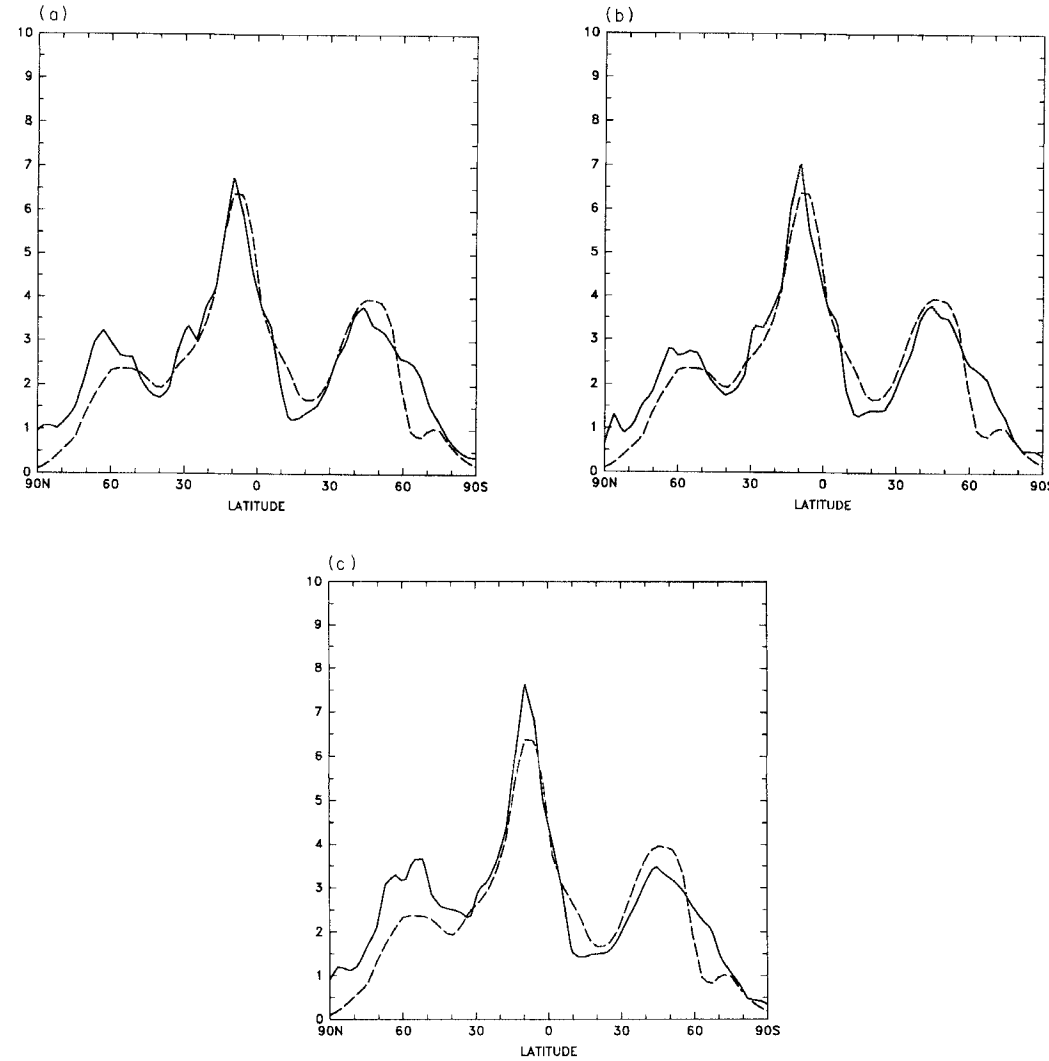

Figure 2. Zonally averaged precipitation rates (mm day^{-1}) for the June–July–August season. Solid lines indicate modelled values, dashed lines observed values. Observations are taken from Jaeger (1976). (a) CLASS: ponded water retained; (b) CLASS: ponded water discarded; (c) old scheme

Looking at the plots of global screen temperature anomalies (Figure 4), it can be seen that there is somewhat more resemblance among the locations and signs of the Northern Hemisphere anomalies generated by the three models than there is in the summer runs. This probably can be attributed to the fact that atmospheric circulations are stronger in the winter, leading to greater persistence of GCM-generated circulation patterns. Measurements taken in remote areas are also likely to be more unreliable in winter, so that some of the observed anomalies may be partly spurious. Large differences in the magnitudes of the anomalies, however, can be assumed to be model-related.

For the old scheme, it is evident that negative anomalies are not quite as widespread as in the season of June–July–August. On the other hand, the magnitudes of anomalies are generally greater. In Northern Hemisphere high latitudes, most of the positive and negative anomalies observed can be attributed to the use of a single layer for soil moisture. The soil thermal model used does not allow surface temperatures to go below 0°C until all of the water in the 'bucket' is frozen. This leads to two results: first, the transition period to

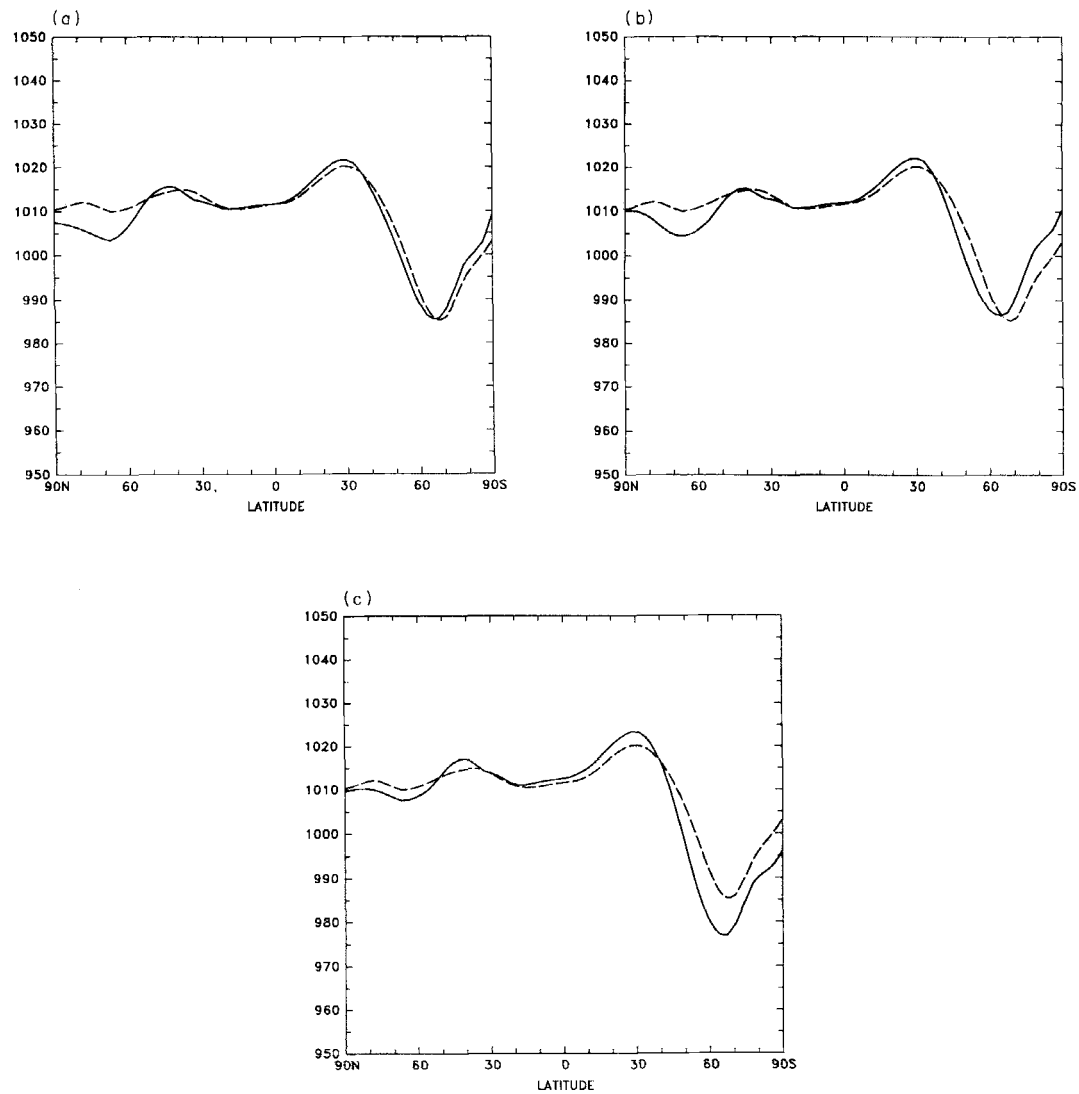

Figure 3. Zonally averaged mean sea-level pressure (hpa) for the June–July–August season. Solid lines indicate modelled values, dashed lines observed values. Observations are NMC 10-year climatological values. (a) CLASS: ponded water retained; (b) CLASS: ponded water discarded; (c) old scheme

Table III. Global average values of surface fields: December– January–February

	Whole globe		Land only	
	Screen temperature (°C)	Precipitation rate (mm day^{-1})	Screen temperature (°C)	Precipitation rate (mm day^{-1})
Observed	12·4	2·8	2·9	1·9
CLASS—ponded water retained	12·5	2·9	2·5	2·6
CLASS—ponded water discarded	12·5	2·8	2·6	2·5
Old scheme	11·6	2·9	−0·1	2·8

subfreezing surface temperatures is artificially prolonged, and second, once the soil water has frozen completely, the surface temperature plunges quickly to unrealistically low values. (These effects are not observed in CLASS, firstly because surface temperatures are allowed to pass below 0°C before even the first soil layer is entirely frozen, and secondly because the existence of unfrozen lower layers sets up a surfaceward ground heat flux, damping the response of the surface temperature to environmental forcing.) Thus, in very

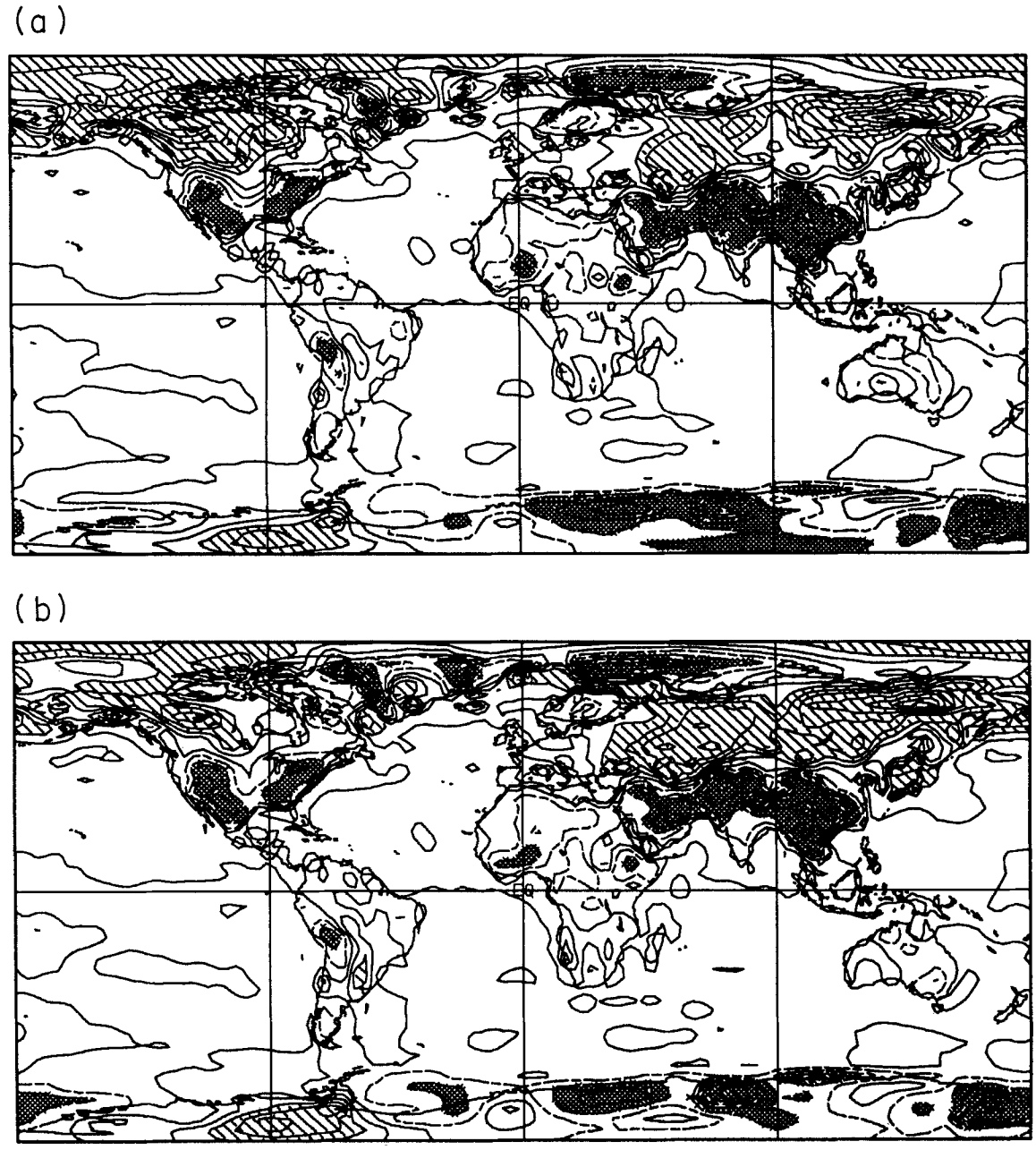

Figure 4. Global screen temperature (°C) anomaly plots (modelled–observed) for the December–January–February season. Diagonal shading indicates values greater than 4°C and cross-hatching values less than −4°C. Contour interval is 2°C; dashed contours indicate negative values. Observed fields were supplied by NCAR. (a) CLASS: ponded water retained; (b) CLASS: ponded water discarded; (c) old scheme

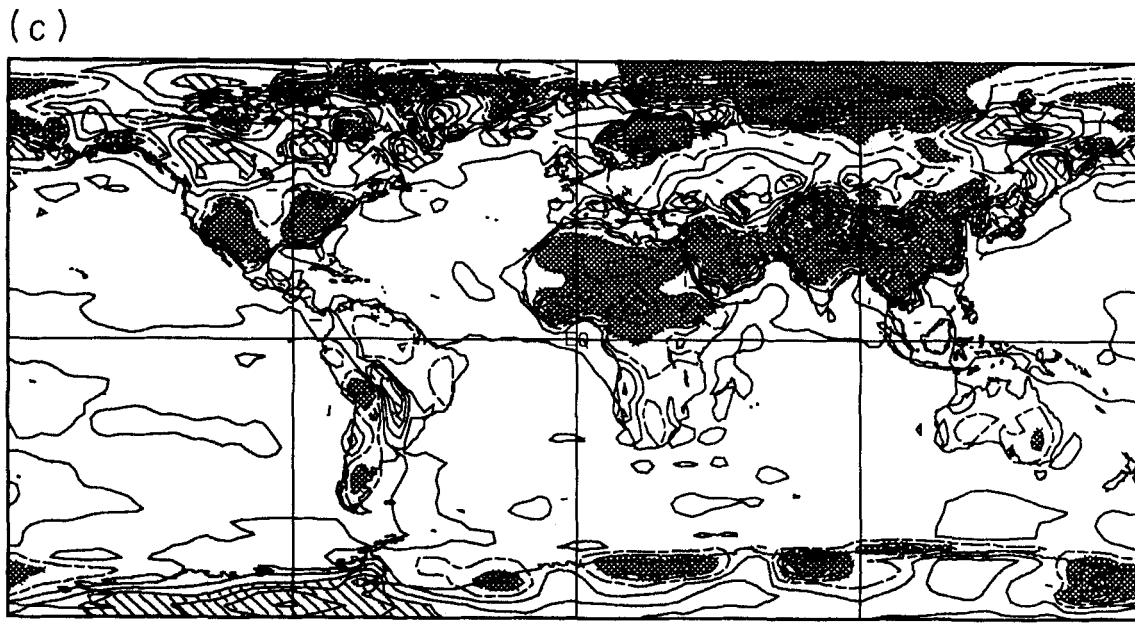

Figure 4. (Continued)

cold regions, such as north-central Siberia, the strongly negative surface forcing causes the transition period to subzero surface temperatures to be fairly short, and temperatures to drop quickly to very low levels. Where the surface forcing is not as strong, as in central Canada and south-western Asia, the effect of the 0°C transition period dominates, leading to positive temperature anomalies.

The most serious temperature underestimation observed is in southern Asia, where the magnitude of the anomaly exceeds 20°C in places. Over India and south-east Asia the low temperatures are probably caused by the neglect of vegetation stomatal resistance, whose effects were noted in section 3.1. The anomaly is more severe than in June–July–August in this particular area, because the occurrence of the Asian monsoon during the summer months probably causes evaporation to proceed at close to the potential rate, since the stomatal resistance associated with wet canopies is zero. Over the Himalayas and the Gobi Desert, the use of the force-restore method again leads to negative temperature anomalies, as described in section 3.1. The same effect is observed over the Sahara and the Middle East.

Large positive anomalies are observed over north-western Canada and eastern Siberia. These are also found in the runs done using CLASS, however, which suggests, as concluded in section 3.1, that the cause is not directly related to the formulation of the models. Again, it seems that the anomalies are produced by a flaw in the characterization of the local vegetation. The two areas in question are covered by boreal forest, to which CLASS assigns canopy parameters corresponding to the values associated with coniferous trees, taken from the literature. However, most of the studies from which these values were obtained were carried out in temperate forests, which are considerably taller and denser than their boreal counterparts. Thus, in winter it is likely that the boreal forests in CLASS are masking the underlying snow cover more than they should, leading to decreased surface albedo. This hypothesis will be tested using data collected during the upcoming BOREAS experiment.

Comparing the results generated by the two versions of CLASS, it can be seen that while both perform well in the tropics and in the Southern Hemisphere, large positive anomalies are associated with central Asia as well as with north-western Canada and eastern Siberia. The first anomaly is probably related to a problem with the stomatal resistance formulation, as noted in June–July–August. The magnitude of the anomaly is much larger in the run in which ponded surface water is discarded as runoff; this again points to the conclusion that making this assumption results in serious errors in modelled surface temperatures. The

second and third anomalies, while partly explained by the snow masking problem outlined above, are substantially worse in the run in which ponded water is retained. This can be attributed to a problem that arises when the latter version of the model is used in areas underlain by permafrost. In such regions, the surface infiltration and evaporation rates are both very low, with the result that the snow meltwater produced in the spring does not disappear by the following winter. Consequently, when winter arrives this stored water gradually refreezes, releasing latent heat which artificially raises the surface temperature. This problem is currently being circumvented by specifying a maximum ponding depth, but it is clear that some parameterization of surface runoff will have to be developed in the future in order to provide a permanent solution.

In Figure 5, zonally averaged values of precipitation are presented for the three runs and compared with observations. Much the same pattern is evident as in the June–July–August season. The old scheme, as before, generates too much precipitation over the Northern Hemisphere and the tropics, because of its tendency to overestimate land surface evaporation; the magnitude of the Northern Hemisphere anomaly is

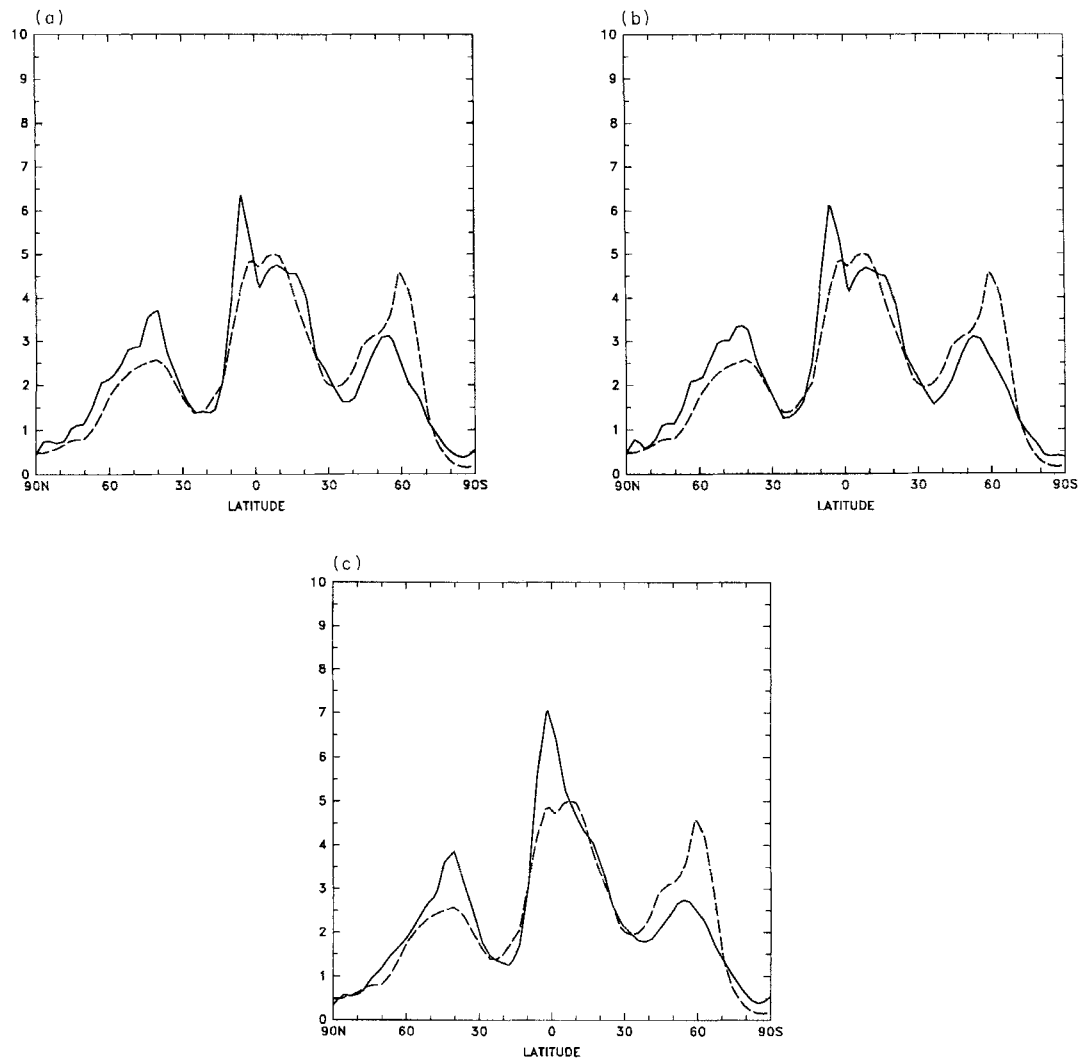

Figure 5. Zonally averaged precipitation rates (mm day^{-1}) for the December–January–February season. Solid lines indicate modelled values, dashed lines observed values. Observations are taken from Jaeger (1976). (a) CLASS: ponded water retained; (b) CLASS: ponded water discarded; (c) old scheme

smaller than in the summer because of generally lower evaporation rates. The depression of land surface temperatures again leads to negative precipitation anomalies in the Southern Hemisphere. For the two runs done using CLASS, it can be seen that the prolonged surface water storage in the Northern Hemisphere leads to precipitation anomalies at 40–45°N that are actually similar in magnitude to those obtained using the old scheme.

Finally, zonally averaged mean sea-level pressures for the three runs and for observations are shown in Figure 6. As in June–July–August, positive screen temperature anomalies in both versions of CLASS lead to underestimates of surface pressure at northern high latitudes; on the other hand, this effect is again mitigated in the old scheme by the extensive negative screen temperature anomalies generated, particularly over northern Asia. The predominance of low screen temperatures in the old scheme also leads to unrealistically high surface pressures in the tropics. Over Antarctica and the adjacent subpolar ocean, on the other hand, negative coastal screen temperature anomalies lead to negative surface pressure anomalies, as explained in section 3.1 above.

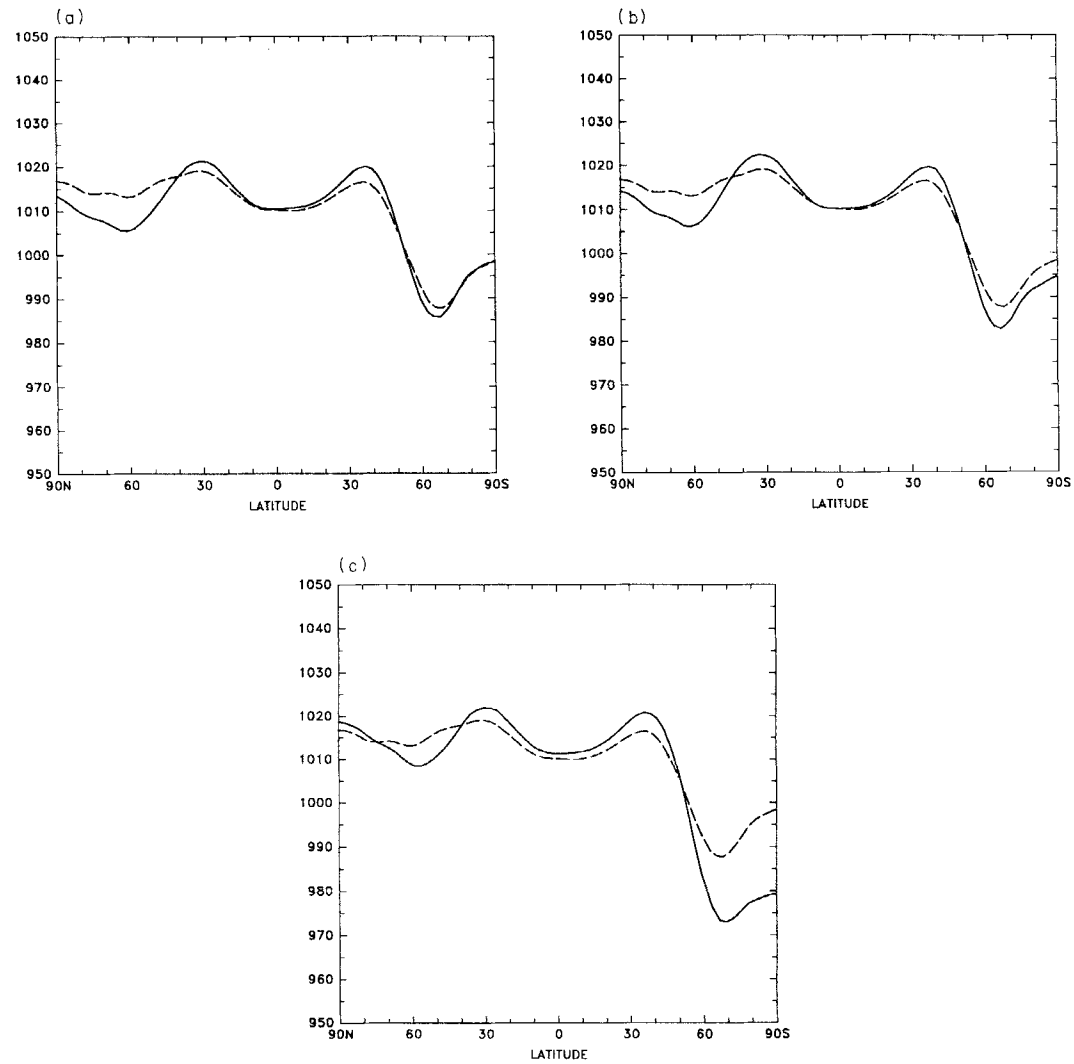

Figure 6. Zonally averaged mean sea-level pressure (hpa) for the December–January–February season. Solid lines indicate modelled values, dashed lines observed values. Observations are NMC 10-year climatological values. (a) CLASS: ponded water retained; (b) CLASS: ponded water discarded; (c) old scheme

4. SUMMARY AND CONCLUSIONS

The vegetation model associated with CLASS has been outlined, and its linkages with the soil model introduced in Part I have been described. The strategies used in coupling CLASS to the Canadian Climate Centre GCM have been discussed. The results of a set of test runs have been presented, with the performance of two versions of CLASS being evaluated against that of the older, simpler land surface scheme previously used in the GCM.

The results of the test runs clearly show that the old scheme generates a land surface climate that is considerably too cold and too wet compared with observations. It is argued that in the tropics and in the summer hemisphere, this is primarily caused by the neglect of vegetation stomatal resistances to transpiration. Negative temperature anomalies in winter high latitudes are apparently caused by freezing of the single subsurface soil layer assumed by the bucket model. Summer overestimations and winter underestimations of bare-soil temperatures in desert areas are traced to the neglect of annual-scale forcing from deeper soil layers. (This drawback of the force-restore method was also noted in Verseghy (1991).)

The results generated by CLASS are characterized by considerably smaller temperature and precipitation anomalies. It is postulated that the largest observed screen temperature anomalies are caused by shortcomings in the modelling of the morphological characteristics of vegetation, owing to lack of field data. One of the most important conclusions drawn from this study is that the assumption made in most GCMs that excess surface water is immediately lost to runoff can lead to substantial positive screen temperature anomalies in continental interiors.

A number of improvements still remain to be made to CLASS. Some of these were already recognized in Verseghy (1991). Parameterizations will have to be developed for overland runoff and lateral ground-water flow, particularly in areas underlain by permafrost. Testing of CLASS against the comprehensive data provided by large-scale field experiments, such as HAPEX-MOBILHY, FIFE, BOREAS, etc., will have to be carried out to check and improve parameterizations, particularly those concerned with vegetation characteristics, such as stomatal resistance, snow masking effects, and drought-related variations in albedo and leaf area index. Finally, some ways of improving the modelling of subgrid-scale variability of convective precipitation and surface soil moisture may have to be sought: perhaps along the lines of the work of Warrilow *et al.* (1986), Wetzel and Chang (1988) and Entekhabi and Eagleson (1989). The division of each grid square into four subareas admittedly provides no more than a first approximation to the solution of this problem. Despite the fledgling state of CLASS, however, the present study clearly indicates that it provides a much more realistic simulation of land surface climates than does a simple 'force-restore *cum* bucket' type of model.

REFERENCES

Abramopoulos, F., Rosenzweig, C. and Choudhury, B. 1988. 'Improved ground hydrology calculations for global climate models (GCMs): Soil water movement and evapotranspiration', *J. Climate*, **1**, 921–941.

Avissar, R., Avissar, P., Mahrer, Y. and Bravdo, B. A. 1985. 'A model to simulate response of plant stomata to environmental conditions', *Agric. For. Meteorol.*, **34**, 21–29.

Avissar, R. and Pielke, R. A. 1989. 'A parameterization of heterogeneous land surfaces for atmospheric numerical models and its impact on regional meteorology', *Mon. Wea. Rev.*, **117**, 2113–2136.

Brutsaert, W. 1979. 'Heat and mass transfer to and from surfaces with dense vegetation or similar permeable roughness', *Boundary-Layer Meteorol.*, **16**, 365–388.

Carlson, T. N., Perry, E. M. and Schmugge, T. J. 1990. 'Remote estimation of soil moisture availability and fractional vegetation cover for agricultural fields', *Agric. For. Meteorol.*, **52**, 45–69.

Carson, D. J. 1986. *Parametrizations of Land-suface Processes in Meteorological Office Numerical Weather Prediction and Climate Models*, Meteorological Office, Bracknell, DCTN 37, 54 pp.

Deardorff, J. W. 1972. 'Parameterization of the planetary boundary layer for use in general circulation models', *Mon. Wea. Rev.*, **100**, 93–106.

Deardorff, J. W. 1978. 'Effective prediction of ground surface temperature and moisture, with inclusion of a layer of vegetation', *J. Geophys. Res.*, **83**(C4), 1889–1903.

Dickinson, R. E., Henderson-Sellers, A., Kennedy, P. J. and Wilson, M. F. 1986. *Biosphere–Atmosphere Transfer Scheme (BATS) for the NCAR Community Climate Model*, National Centre for Atmospheric Research, Boulder, Colorado, NCAR/TN-275+STR, 69 pp.

Entekhabi, D. and Eagleson, P. S. 1989. 'Land surface hydrology parameterization for atmospheric general circulation models including subgrid scale variability', *J. Climate*, **2**, 816–831.

Feddes, R. A., Bresler, E. and Neuman, S. P. 1974. 'Field test of a modified numerical model for water uptake by root systems', *Water Resour. Res.*, **10,** 1199–1206.
Federer, C. A. 1979. 'A soil–plant–atmosphere model for transpiration and availability of soil water', *Water Resour. Res.*, **15,** 555–562.
Garratt, J. R. and Hicks, B. B. 1973. 'Momentum, heat and water vapour transfer to and from natural and artificial surfaces', *Q. J. R. Meteorol. Soc.*, **99,** 680–687.
Gash, J. H. C. 1979. 'An analytical model of rainfall interception by forests', *Q. J. R. Meteorol. Soc.*, **105,** 43–55.
Goudriaan, J. 1988. 'The bare bones of leaf-angle distribution in radiation models for canopy photosynthesis and energy exchange', *Agric. For. Meteorol.*, **43,** 155–169.
Hancock, N. H. and Crowther, J. M. 1979. 'A technique for the direct measurement of water storage on a forest canopy', *J. Hydrol.*, **41,** 105–122.
Jaeger, L. 1976. *Monatskarten des Niederschlags für die ganze Erde*, Bericht Deutscher Wetterdienst 18, No. 139, 38 pp.
Leonard, R. E. and Eschner, A. R. 1968. 'Albedo of intercepted snow', *Water Resour. Res.*, **4,** 931–935.
Mahfouf, J-F. and Jacquemin, B. 1989. 'A study of rainfall interception using a land surface parameterization for mesoscale meteorological models', *J. Appl. Meteorol.*, **28,** 1282–1302.
Mahrt, L. 1987. 'Grid-averaged surface fluxes', *Mon. Wea. Rev.*, **115,** 1550–1560.
McFarlane, N. A., Boer, G. J., Blanchet, J-P. and Lazare, M. 1992. 'The Canadian Climate Centre second generation general circulation model and its equilibrium climate', *J. Climate*, **5,** 1013–1044.
Meehl, G. A. and Washington, W. M. 1988. 'A comparison of soil moisture sensitivity in two global climate models', *J. Atmos. Sci.*, **45,** 1476–1492.
Monteith, J. L. 1965. 'Evaporation and environment', *Symp. Soc. Explor. Biol.*, **19,** 205–234.
Noilhan, J. and Planton, S. 1989. 'A simple parameterization of land surface processes for meteorological models', *Mon. Wea. Rev.*, **117,** 536–549.
Radcliffe, D., Hayden, T., Watson, K., Crowley, P. and Phillips, R. E. 1980. 'Simulation of soil water within the root zone of a corn crop', *Agron. J.*, **72,** 19–24.
Rutter, A. J., Kershaw, K. A., Robins, P. C. and Morton, A. J. 1971. 'A predictive model of rainfall interception in forests, I. Derivation of the model from observations in a plantation of Corsican pine', *Agric. Meteorol.*, **9,** 367–384.
Sato, N., Sellers, P. J., Randall, D. A., Schneider, E. K., Shukla, J., Kinter, J. L. III, Hou, Y-T. and Albertazzi, E. 1989. 'Effect of implementing the simple biosphere model in a general circulation model', *J. Atmos. Sci.*, **46,** 2757–2782.
Sellers, P. J., Mintz, Y., Sud, Y. C. and Dalcher, A. 1986. 'A simple biosphere model (SiB) for use within general circulation models', *J. Atmos. Sci.*, **43,** 505–531.
Sherratt, D. J. and Wheater, H. S. 1984. 'The use of surface resistance–soil moisture relationships in soil water budget models', *Agric. For. Meteorol.*, **31,** 143–157.
Simpson, J. R., Fritschen, L. J. and Walker, R. B. 1985. 'Estimating stomatal diffusion resistance for Douglas fir, lodgepole pine and white oak under light saturated conditions', *Agric. For. Meteorol.*, **33,** 299–313.
Steven, M. D. and Unsworth, M. H. 1980. 'The angular distribution and interception of diffuse solar radiation below overcast skies', *Q. J. R. Meteorol. Soc.*, **106,** 57–61.
Stewart, J. B. 1988. 'Modelling surface conductance of pine forest', *Agric. For. Meteorol.*, **43,** 19–35.
Sud, Y. C., Sellers, P. J., Mintz, Y., Chou, M. D., Walker, G. K. and Smith, W. E. 1990. 'Influence of the biosphere on the global circulation and hydrological cycle—a GCM simulation experiment', *Agric. For. Meteorol.*, **52,** 133–180.
Taconet, O., Bernard, R. and Vidal-Madjar, D. 1986. 'Evapotranspiration over an agricultural region using a surface flux/temperature model based on NOAA- AVHRR data', *J. Clim. Appl. Meteorol.*, **25,** 284–307.
Taylor, P. A. 1987. 'Comments and further analysis on effective roughness lengths for use in numerical three-dimensional models', *Boundary-Layer Meteorol.*, **39,** 403–418.
Thom, A. S. and Oliver, H. R. 1977. 'On Penman's equation for estimating regional evaporation', *Q. J. R. Meteorol. Soc.*, **103,** 345–357.
Tjernström, M. 1989. 'Some tests with a surface energy balance scheme, including a bulk parameterisation for vegetation, in a mesoscale model', *Boundary-Layer Meteorol.*, **48,** 33–68.
Townsend, A. A. 1964. 'Natural convection in water over an ice surface', *Q. J. R. Meteorol. Soc.*, **90,** 248–259.
Verseghy, D. L. 1991. 'CLASS—A Canadian land surface scheme for GCMs, I. Soil model', *Int. J. Climatol.*, **11,** 111–133.
Warrilow, D. A., Sangster, A. B. and Slingo, A. 1986. *Modelling of Land Surface Processes and their Influence on European Climate*, Meteorological Office, Bracknell, DCTN 38, 92 pp.
Wetzel, P. J. and Chang, J-T. 1988. 'Evapotranspiration from nonuniform surfaces: a first approach for short-term numerical weather prediction', *Mon. Wea. Rev.*, **116,** 600–621.
Wilson, M. F. and Henderson-Sellers, A. 1985. 'A global archive of land cover and soils data for use in general circulation climate models', *J. Climatol.*, **5,** 119–143.